

1 © IWA Publishing [2018]. The definitive peer-reviewed and edited version of this
2 article is published in the *Journal of Hydroinformatics*, 2018, 20 (3): 564-576,
3 <https://doi.org/10.2166/hydro.2018.127> and is available at www.iwapublishing.com

4 **Surface to sewer flow exchange through circular inlets during urban**
5 **flood conditions**

6 Matteo Rubinato, Seungsoo Lee, Ricardo Martins and James D.

7 Shucksmith

8 **Matteo Rubinato**

9 **Ricardo Martins**

10 **James D. Shucksmith**

11 The University of Sheffield, Civil and Structural Engineering Department, Sir Frederick
12 Mappin Building, Mappin Street, S1 3JD, Sheffield, UK

13 **Seungsoo Lee** (corresponding author)

14 APEC Climate Center, 12 Centum 7-ro, Haeundae-gu, Busan, 612-020, Republic of
15 Korea, 48058

16 E-mail: seungsoo_lee@apcc21.org

17 **Ricardo Martins**

18 MARE - Marine and Environmental Sciences Centre, Department of Civil Engineering,
19 FCT, University of Coimbra, Coimbra, Portugal

20 **Ricardo Martins**

21 IMAR - Institute of Marine Research, FCT, University of Coimbra, Coimbra, Portugal

22

23 **ABSTRACT**

24 Accurately quantifying the capacity of sewer inlets (such as manhole lids and
25 gullies) to transfer water is important for many hydraulic flood modelling tools.

26 The large range of inlet types and grate designs used in practice makes the

27 representation of flow through and around such inlets challenging. This study uses
28 a physical scale model to quantify flow conditions through a circular inlet during
29 shallow steady state surface flow conditions. Ten different inlet grate designs have
30 been tested over a range of surface flow depths. The resulting datasets have been
31 used (i) to quantify weir and orifice discharge coefficients for commonly used
32 flood modelling surface–sewer linking equations; (ii) to validate a 2D finite
33 difference model in terms of simulated water depths around the inlet. Calibrated
34 weir and orifice coefficients were observed to be in the range 0.115–0.372 and
35 0.349–2.038, respectively, and a relationship with grate geometrical parameters
36 was observed. The results show an agreement between experimentally observed
37 and numerically modelled flow depths but with larger discrepancies at higher flow
38 exchange rates. Despite some discrepancies, the results provide improved
39 confidence regarding the reliability of the numerical method to model surface to
40 sewer flow under steady state hydraulic conditions.

41 **Key words** | experimental modelling, numerical modelling, surface to
42 sewer flow exchange, urban flooding, discharge coefficients

43 INTRODUCTION

44 Current climatic trends mean that the frequency and magnitude of urban
45 flooding events is forecast to increase in the future (Hammond *et al.* 2015) leading to
46 increased damage in terms of loss of business, livelihoods plus increased inconvenience
47 for citizens (Ten Veldhuis & Clemens 2010). These potential impacts underline the
48 importance of accurate modelling tools to determine flow paths within and between
49 overland surfaces and sewer/drainage systems. Existing urban flood models commonly
50 utilise the 1D Saint-Venant and 2D Shallow Water Equations (SWE) to calculate flows
51 within sewer pipes and on the surface (overland flow) (Martins *et al.* 2017b). However,
52 modelers are also faced with the concern of how to correctly reproduce the hydraulic
53 behaviour around and within complex and variable hydraulic structures such as
54 manholes and gullies which are used to connect the surface system to the sewer system.
55 Unless the inlet is blocked or the sewer is surcharged, these structures allow water to be
56 drained from the surface. An inaccurate representation of inlet capacity can lead to
57 incorrect prediction of flow volumes, velocities and depths on the surface (Xia *et al.*

2017), as well as in the sewer pipes. Due to their geometrical complexity such linking structures are conventionally represented using weir and orifice equations within urban flood models (Djordjevic' *et al.* 2005; Chen *et al.* 2007; Leandro *et al.* 2009; Martins *et al.* 2017a). However, due to a paucity of datasets, the robust calibration and validation of such linking methodologies is lacking. In particular, the determination of appropriate discharge coefficients for such linking equations over a range of hydraulic conditions and inlet types is required. Experimental studies investigating surface–sewer flow interaction via gullies and manholes are scarce (Martins *et al.* 2014). Larson (1947) identified inlet width and the efficiency of the inlet opening as characteristics of primary importance to determine inlet capacity; Li *et al.* (1951, 1954) experimentally investigated the effectiveness of some grate inlets in transferring flow from surface to sewer by treating the flow bypassing the grate as separate portions, and Guo (2000a, 2000b) and Almedeij & Houghtalen (2003), proposed different modifications to grate inlet design. Gómez & Russo (2009) investigated the hydraulic efficiency of transverse grates within gully systems proposing new mathematical expressions to define the hydraulic efficiency. Gómez & Russo (2011a) studied the hydraulic behaviour of inlet grates in urban catchments during storm events and Gómez *et al.* (2011b) presented an empirical relationship to obtain the hydraulic efficiency as a function of inlet and street flow characteristics. In further work, Gómez *et al.* (2013) investigated the hydraulic efficiency reduction as a result of partially clogged grate inlets. More recently, Rubinato *et al.* (2017a) experimentally validated the ability of weir/orifice linking equations to represent steady flow exchange through a scaled open manhole. However, the performance was dependent on the calibration of the discharge coefficients as well as a robust characterisation of the flow within the sewer and flow depth on the surface such that the hydraulic head difference between surface and sewer flows could be accurately determined. An accurate representation of flow exchange is therefore also dependent on correctly modelling of flow conditions (hydraulic head) in the vicinity of the inlet structure. Literature published to date lacks repeatable tests of different grate inlets under controlled conditions and an integration of results into modelling tools. Numerical studies of flows around gullies and manholes are limited due to a lack of experimental data as well as long computational times when simulating complex 3D flows (Leandro *et al.* 2014). However, some studies have been conducted: Lopes *et al.* (2015) analysed experimental results from a surcharging jet arising from the reverse flow out of a manhole after the sewer system became pressurised; Djordjevic' *et al.*

92 (2013) focused on surface recirculation zones formed downstream of gullies; both
93 studies have used experimental data to model flow patterns inside gullies and manholes
94 using CFD; Rubinato *et al.* (2016) studied flow depths around an open circular manhole
95 under drainage conditions and validated a 2D finite difference model. Martins *et al.*
96 (2017a) validated two finite volume (FV) flood models in the case where horizontal
97 floodplain flow is affected by sewer surcharge flow via a manhole demonstrating that
98 the shock capturing FV-based flood models are applicable tools to model localised
99 sewer-to-floodplain flow interaction. However, no studies to date have looked
100 specifically at the influence of different grate cover designs/geometries on flow
101 exchange capacity, flow conditions around the inlet and the ability of 2D modelling
102 tools to replicate depths around the inlet over a range of flows. The objective of this
103 work is to use a physical scale model to collect an extensive series of experimental
104 datasets describing surface to sewer flow exchange through a circular inlet under steady
105 state conditions through ten different inlet grate configurations. The datasets are used to
106 (i) determine appropriate weir/orifice discharge coefficients applicable to describe
107 exchange flows and (ii) to validate the ability of a calibrated 2D numerical finite
108 difference method (FDM) to describe observed surface flow depths in the vicinity of the
109 inlet structure.

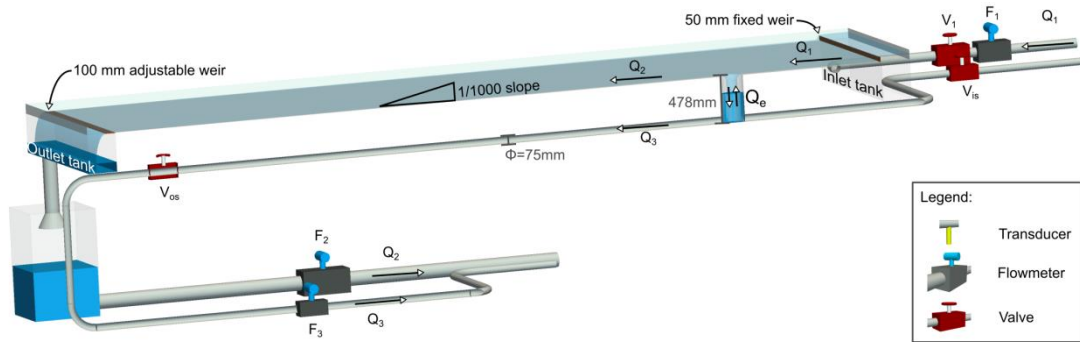
110 **METHODOLOGY**

111 This section presents (i) the experimental facility used to collect the data, (ii) hydraulic
112 conditions for the tests conducted, (iii) a detailed procedure of the methods used to
113 estimate discharge coefficients of the linking equations and (iv) a description of the
114 numerical flood model utilised.

115 **Experimental model**

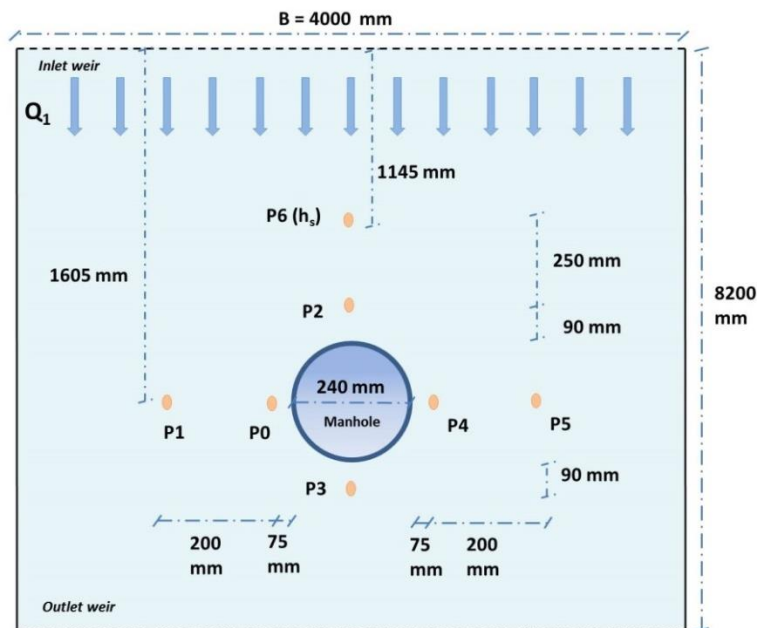
116 The experimental set-up utilised (Figure 1) was assembled at the water laboratory of the
117 University of Sheffield (UK) (Rubinato 2015). It consists of a scaled model of an urban
118 drainage system/floodplain linked via a manhole shaft. The floodplain surface (4 m,
119 width, by 8.2 m, length) has a longitudinal slope of 1/1000. The urban drainage system
120 is made from horizontal acrylic pipes directly beneath the surface (inner diameter =
121 0.075 m). One circular acrylic shaft (representing a manhole) with 0.240 m inner
122 diameter and 0.478 m height connects the surface to the pipes. The facility is equipped

123 with a SCADA system (Supervision, Control and Data Acquisition) through Labview™
 124 software that permits the setup and monitoring of flow rates within the surface and
 125 sewer systems independently. A pumping system in a closed circuit supplies water
 126 within the facility. The inlet pipes (V_1 , V_{is}) are fitted with electronic control valves
 127 operated via Labview™ software. The surface downstream outlet is a free outfall which
 128 contains an adjustable height weir.



129

130 **Figure 1** | Scheme of the experimental facility (Rubinato *et al.* 2017b).



131

132 **Figure 2** | Location of the pressure transducer measurement points around the surface to
 133 sewer drainage inlet (not to scale).

134 Calibrated electro-magnetic (MAG) flow meters (F_1 , inlet floodplain; F_2 , outlet
 135 floodplain; F_3 outlet sewer) were installed in the upstream and downstream pipes in
 136 order to measure the surface system inflow (Q_1) and surface and sewer outflows (Q_2 ,

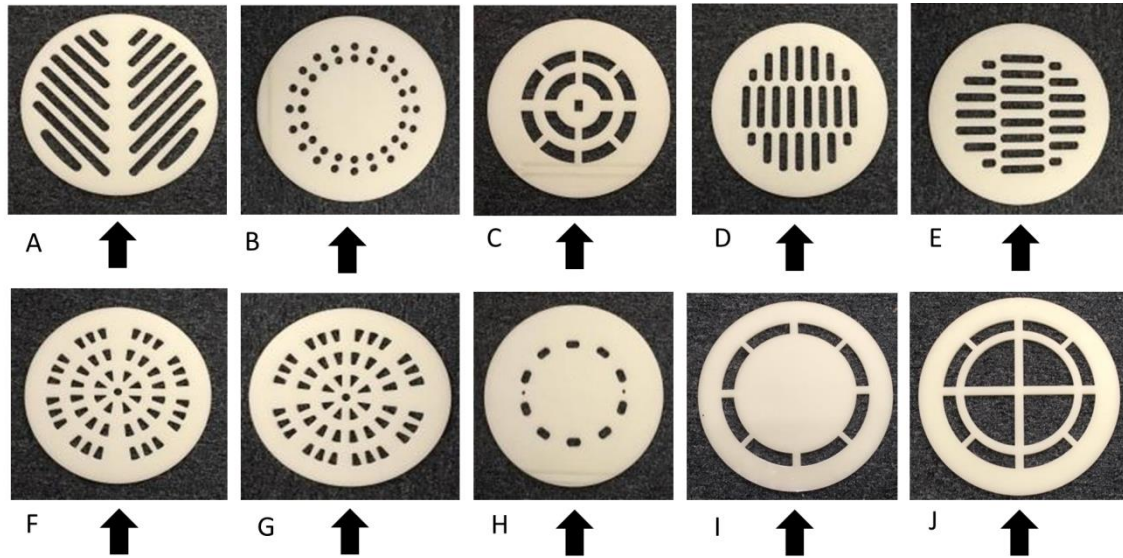
137 Q_3) and calculate the steady state drainage rate through the surface to sewer inlet (Q_e).
138 Each flow meter was independently verified against a laboratory measurement tank. For
139 the tests reported here, the sewer inflow was not used (sewer inflow = 0) and all flow
140 therefore entered the facility via the surface inlet weir (Q_1). Drainage flow passed via
141 the drainage inlet to the sewer outlet ($Q_e = Q_3$), with the remaining flow passing over
142 the facility to downstream outlet weir (Q_2). Flow depth on the floodplain was measured
143 by a series of pressure sensors (of type GEMS series 5000) fitted at various locations
144 around the inlet (Figure 2) (with an accuracy of ± 0.109 mm for the range of water depth
145 0–100 mm). Ten different grate types were constructed from acrylic using a laser cutter
146 and installed within the drainage structure and tested under steady state conditions in
147 order to obtain flow depth vs drainage discharge (Q_e) relationships for each grate type.
148 The grate opening types were selected based on common types used in different
149 countries, and are presented in Figure 3. For each grate opening type the total area of
150 empty space (A_e) and total effective edge perimeter length (P_v) were obtained from the
151 AutoCAD drawings prior to fabrication (Table 1). Autocad drawings are included as
152 supplementary data.

153 **Table 1** | Technical details of the grids utilised

Grate	Area filled A_f (m^2)	Area empty spaces A_e (m^2)	Void ratio V (%)	Effective perimeter P_v (m)
A	0.0307	0.0145	32.1	3.0364
B	0.0421	0.0031	6.9	1.2520
C	0.0373	0.0079	17.48	1.3880
D	0.0353	0.0099	21.9	2.3794
E	0.0353	0.0099	21.9	2.3794
F	0.0391	0.0061	13.5	2.2586
G	0.0391	0.0061	13.5	2.2586
H	0.0435	0.0017	3.76	0.5128

I	0.0385	0.0067	14.11	1.2428
J	0.0277	0.0175	38.03	1.8816

154



155

156

Figure 3 | Grates applied on the top of the inlet (black arrows show the primary direction of the facility inflow Q_1 and hence the orientation of each inlet grate).

157

158

Hydraulic conditions

159

160

161

162

163

164

165

166

167

168

169

170

171

172

For each grate inlet displayed in Figure 3, eight tests have been completed over a range of surface inflows (Q_1) between 4 and 10 l/s set using the upstream valve (V_1). This is equivalent to a unit width discharge ($q_1 = Q_1/B$) between 1 and 2.5 l/s. To ensure reliable depth and flow rate quantification for each test, flows were left to stabilise for 5 minutes before flow rates and depths were recorded. Each reported depth/flow measurement is a temporal average of 3 minutes of recorded data after flow stabilisation, such that full convergence of measured parameters is achieved. In all cases, a flat weir was used as the downstream floodplain boundary, and free surface flow was maintained in the pipe system. The upstream flow depth (h_s) is reported as the depth recorded at transducer P_6 (Figure 2). Surface flow Froude number (Fr) is calculated based on this flow depth and the calculated cross-sectional averaged velocity (U) at this position ($U = Q_1/B \cdot h_s$). The hydraulic conditions for each test are detailed in Table 2. Full (non-averaged) datasets from flow meters Q_1 , Q_3 and transducers (P_0 , P_1 , P_2 , P_3 , P_4 , P_5 , P_6) are presented as supplementary data (Table S1) to this paper.

173

174

175 **Table 2** | Hydraulic parameters measured (Q_I , Q_e and h_s) and calculated (Fr) for the
 176 tests conducted

Grate	Q_I	Q_e	h_s	Fr	Grate	Q_I	Q_e	h_s	Fr
	(l/s)	(l/s)	(mm)	(/)		(l/s)	(l/s)	(mm)	(/)
A	4.33	0.55	7.28	0.556	B	4.29	0.50	7.26	0.554
	5.00	0.67	7.89	0.569		4.99	0.59	7.92	0.565
	5.66	0.76	8.50	0.576		5.67	0.68	8.60	0.568
	6.32	0.86	9.09	0.582		6.33	0.76	9.15	0.577
	6.93	0.93	9.49	0.599		6.93	0.82	9.63	0.586
	7.51	0.94	10.05	0.595		7.52	0.89	10.12	0.590
	8.22	1.05	10.60	0.601		8.18	0.91	10.64	0.596
	9.29	1.19	11.36	0.612		9.22	0.94	11.42	0.603
C	4.29	0.43	7.53	0.524	D	4.23	0.43	7.72	0.498
	4.97	0.54	8.16	0.539		4.96	0.59	8.40	0.514
	5.66	0.63	8.91	0.538		5.69	0.70	9.24	0.512
	6.32	0.72	9.53	0.542		6.30	0.72	10.11	0.495
	6.95	0.74	10.10	0.546		6.96	0.80	10.72	0.501
	7.54	0.80	10.60	0.552		7.49	0.82	11.18	0.506
	8.21	0.88	11.14	0.558		8.19	0.96	11.70	0.516
	9.28	0.97	11.91	0.570		9.24	1.09	12.49	0.529
E	4.27	0.44	7.36	0.540	F	4.28	0.44	7.40	0.537
	5.00	0.53	8.02	0.555		4.95	0.48	8.07	0.545
	5.68	0.63	8.62	0.566		5.66	0.61	8.75	0.552
	6.31	0.69	9.19	0.572		6.37	0.70	9.40	0.558
	6.96	0.77	9.70	0.582		6.96	0.85	9.74	0.577
	7.51	0.81	10.01	0.582		7.52	0.90	10.20	0.582
	8.19	0.90	10.59	0.600		8.17	0.95	10.63	0.595
	9.24	0.99	11.42	0.605		9.25	1.10	11.49	0.599
G	4.22	0.48	7.60	0.508	H	4.26	0.39	7.25	0.551

	4.93	0.61	8.27	0.523		4.97	0.44	7.96	0.558
	5.63	0.72	9.01	0.525		5.66	0.48	8.68	0.559
	6.26	0.80	9.61	0.530		6.29	0.52	9.35	0.555
	6.87	0.84	10.05	0.544		6.92	0.58	9.82	0.567
	7.52	0.94	10.50	0.558		7.51	0.66	10.30	0.574
	8.21	1.03	11.00	0.568		8.19	0.68	10.77	0.584
	9.22	1.13	11.76	0.578		9.22	0.70	11.57	0.592
I	4.26	0.43	7.28	0.547	J	4.26	0.46	7.44	0.530
	4.97	0.57	7.85	0.571		4.94	0.52	8.13	0.538
	5.64	0.63	8.53	0.571		5.66	0.64	8.78	0.549
	6.27	0.71	9.13	0.573		6.27	0.72	9.39	0.550
	6.92	0.78	9.65	0.583		6.91	0.77	9.87	0.562
	7.51	0.88	10.08	0.593		7.52	0.90	10.35	0.570
	8.16	0.93	10.58	0.599		8.18	0.95	10.84	0.579
	9.22	1.03	11.39	0.605		9.21	0.98	11.66	0.584

177

178 *Discharge coefficients*

179 Within flood modelling applications the weir (1) and orifice (2) equations are
180 commonly defined as the following (Rubinato *et al.* 2017a):

$$181 \quad Q_e = \frac{2}{3} C_w \pi D_m \sqrt{2g} (H)^{\frac{3}{2}} \quad (1)$$

182 where D_m is the diameter of the (circular) inlet (m), H is the driving hydraulic head
183 above the interface point accounting for both sewer and surface flows (m). C_w is the
184 weir discharge coefficient.

$$185 \quad Q_e = C_o A_m \sqrt{2gH} \quad (2)$$

186 where A_m is the open area of the inlet and C_o is the orifice coefficient. In cases
187 where the sewer is not surcharged, the hydraulic head (H) is assumed to be equal to the
188 surface flow depth. To calibrate discharge coefficients for each grate type, Equations (2)
189 and (3) were modified to account for the total length of the weir within each grate
190 design (taken as equal to P_v) and total open area (taken as equal to A_e). The flow depth
191 is taken as the measured upstream value (h_s).

$$192 \quad Q_e = \frac{2}{3} C_w P_v \sqrt{2g} (h_s)^{\frac{3}{2}} \quad (3)$$

$$193 \quad Q_e = C_o A_e \sqrt{2g} (h_s)^{\frac{1}{2}} \quad (4)$$

194 **Numerical model**

195 The depth-averaged 2D SWEs are commonly used for modelling flows in urban
 196 environments and in rivers and floodplains (Wang *et al.* 2011). Integrating an inflow
 197 and outflow in/from the sewerage system can be realised by adding suitable source
 198 terms (Lee *et al.* 2013). The governing equations used for floodplain modelling with
 199 surface to sewer inflows are as follows:

$$200 \quad \frac{\partial h}{\partial t} + \frac{\partial(uh)}{\partial x} + \frac{\partial(vh)}{\partial y} = -q_e \quad (5)$$

$$201 \quad \frac{\partial(uh)}{\partial t} + \frac{\partial(u^2h)}{\partial x} + \frac{\partial(uvh)}{\partial y} = -gh \frac{\partial E}{\partial x} - gn^2 \frac{u\sqrt{u^2 + v^2}}{h^{1/3}} \quad (6)$$

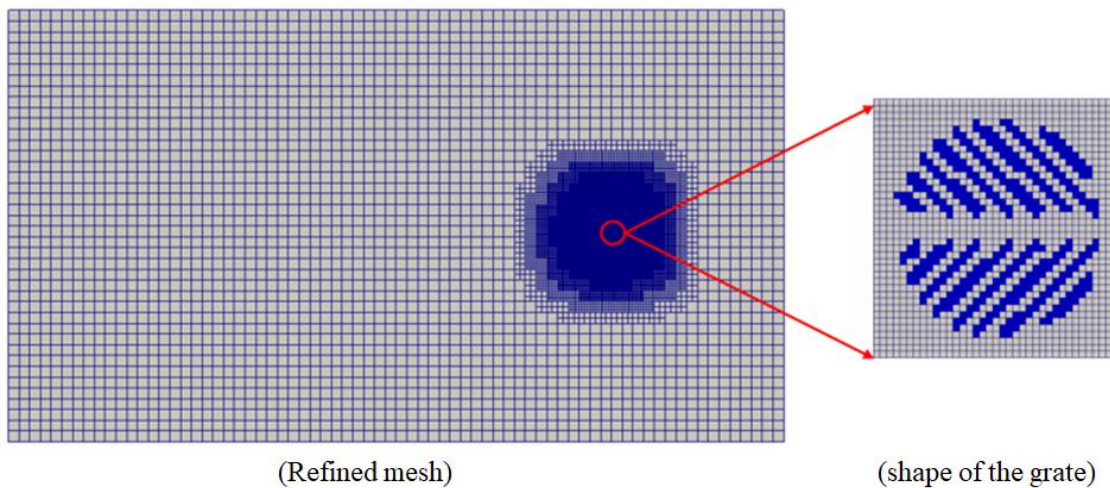
$$202 \quad \frac{\partial(vh)}{\partial t} + \frac{\partial(uvh)}{\partial x} + \frac{\partial(v^2h)}{\partial y} = -gh \frac{\partial E}{\partial y} - gn^2 \frac{v\sqrt{u^2 + v^2}}{h^{1/3}} \quad (7)$$

203 In Equations (5)–(7), (x, y) are the spatial Cartesian coordinates and t is the time (SI
 204 units). h (m) is the water depth u and v (m/s) are x- and y-direction velocities,
 205 respectively. E is the water elevation (m), and n is Manning's roughness coefficient
 206 (here taken as 0.009 m/s^{1/3}, from previous experimental work, e.g., Rubinato *et al.*
 207 (2017a)). q_e (m/s) is the area discharge, in this study representing surface to sewer
 208 discharge via the inlet grate. A leap-frog method is used in order to reduce simulation
 209 time, with variables laid on staggered mesh. Fluxes (uh and vh) are located at the
 210 computational cell boundary and water depth (h) is located at the centre of the
 211 computational cell. More detailed information regarding the leap-frog and FDM
 212 methods can be found in Lee (2013).

213 *Model setup and boundary conditions*

214 An adaptive mesh technique (Haleem *et al.* 2015) is used to reduce the calculation time (Figure
 215 4). In the simulation, the downstream depth measurement point (P₇) is used to define
 216 downstream boundary conditions, hence the initial number of quadrilaterals was chosen to be 72
 217 × 40 (7.2 m × 4.0 m) to generate a baseline (coarse) mesh with a spatial resolution of around 0.1
 218 m × 0.1 m. A mesh convergence analysis was carried out, which suggested the need for a four
 219 times finer mesh for the model to be able to appropriately resolve the hydrodynamics of the
 220 grate inlet. As shown in Figure 4, up to four levels of refinement are implemented around the

221 local zone of sewer-to-floodplain interaction (resolution around $6.25 \text{ mm} \times 6.25 \text{ mm}$) and these
222 are assumed appropriate to replicate the geometry of each grate type. The open cells within each
223 grate area are identified as cells where the q_e term in Equation (5) is nonzero. The total flow
224 exchange from surface to sewer is calculated by applying Equation (3) using the experimentally
225 obtained weir coefficients and simulated upstream water depth at P_6 (h_s). q_e for each open cell is
226 then calculated based on the total calculated flow exchange and the total open area of each grate
227 type. All the simulations were run until convergence to a steady state is attained. A mesh
228 convergence analysis suggested the use of a convergence (depth) threshold-error no bigger than
229 10^4 and no less than 10^6 . The initial discharge condition is taken to be the unit width surface
230 inflow q_1 and a measured velocity profile is used to set water depth at the eastern (upstream)
231 boundary. This velocity curve was obtained prior to the experiments by measuring ten flows
232 (Q_1) between 2 l/s and 11 l/s and recording the average velocity in the area included between
233 0.5 and 3.5 m of the total width, with sampling points each 0.5 m. At the southern and northern
234 boundaries (lateral), a wall boundary condition is employed (reflective). At the western
235 (downstream) boundary, measured water depth at P_7 is used.



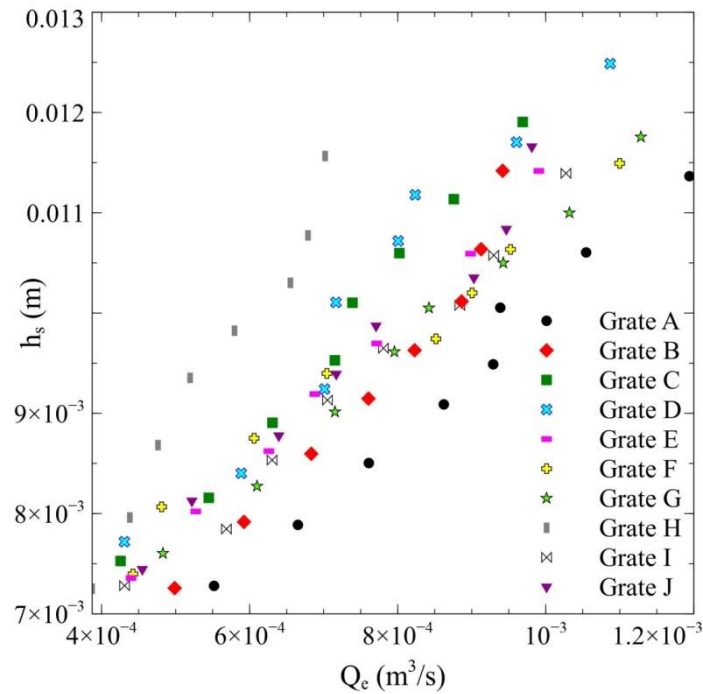
236 (Refined mesh) (shape of the grate)
237 **Figure 4** | Mesh characterisation example for grate type A.

238 RESULTS AND DISCUSSIONS

239 This section presents discharge coefficients estimated for each grate configuration and
240 the comparison of the 2D finite difference model predictions against observed flow
241 depths recorded around the inlet at seven different pressure sensor locations (P_0 – P_6)
242 displayed in Figure 2.

243 **Experimental results and calibrated discharge coefficients**

244 Figure 5 shows the relationship between the upstream water depth (h_s) and the
245 correspondent flow exchange (Q_e) through each grate type over the range of flow
246 conditions tested.



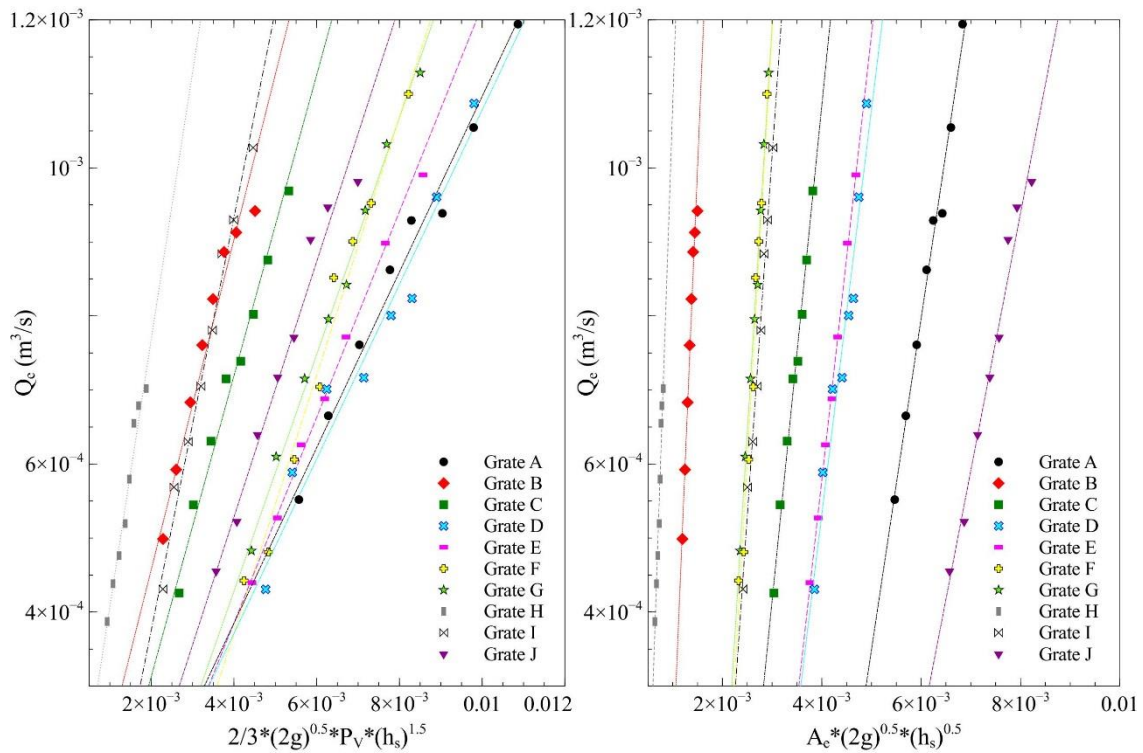
247

248 **Figure 5** | The observed relationship between upstream water depth vs surface to sewer
249 flow exchange for each grate type.

250 The results confirm that the geometry of each grate strongly influences the flow
251 entering the surface-sewer inlet. When comparing results for similar hydraulic
252 conditions, grate H ($A_e = 0.0017 \text{ m}^2$; $P_v = 0.5128 \text{ m}$) is the grate that results in the
253 lowest exchange flows while grate A allows the highest exchange flows ($A_e = 0.0145$
254 m^2 ; $P_v = 3.0364 \text{ m}$). It can be noted that while grate A has the highest perimeter values,
255 its void area is lower than grate J. In general, the results confirm that the exchange flow
256 capacity of each grate design is more strongly correlated to the effective perimeter than
257 the void area; however, individual different grate designs can affect the flow patterns
258 around the void spaces and hence drainage efficiency. To provide a better understanding
259 of this a further investigation including consideration of the local flow velocity is
260 required.

261 Calibration of Equations (3) and (4) is achieved by fitting a linear trend between the
262 terms of the relevant equation and the surface to sewer exchange flow (Q_e) for each
263 grate type (shown in Figure 6). The average goodness of fit of the linkage equations

264 over all grate types (weir equation average $R^2 = 0.977$, orifice equation $R^2 = 0.980$)
 265 shows that both weir and orifice equations are shown to be applicable for representation
 266 of surface to sewer flow exchange in steady flow (confirming previous work, Rubinato
 267 *et al.* (2017a)) and that over the range of hydraulic conditions tested here, the weir and
 268 orifice coefficients can be taken as constant. Calibrating the weir Equation (3) against
 269 the experimental results provides a discharge coefficient C_w in the range 0.115–0.372
 270 based on the variety of grates applied (Table 1). Calibration of the orifice Equation (4)
 271 against the experimental results provides a discharge coefficient C_o in the range 0.349–
 272 2.038. Values for each grate type are provided in Table 3, along with correspondent
 273 goodness of fit values (R^2). Discharge coefficients observed in this study are in the same
 274 range to those found by Martins *et al.* (2014) for a $0.6 \times 0.3 \times 0.3$ m gully under
 275 drainage conditions ($0.16 < C_w < 1.00$, $1.36 < C_o < 2.68$) but differs to those obtained by
 276 Bazin *et al.* (2014) for small (0.05×0.05 m) fully open street inlets ($0.58 < C_o < 0.67$).
 277 This is likely due to the variation in scales between the experimental facilities used. It is
 278 noticeable that the orifice equation results in a larger variation in the range of calibrated
 279 coefficients than the weir equation.



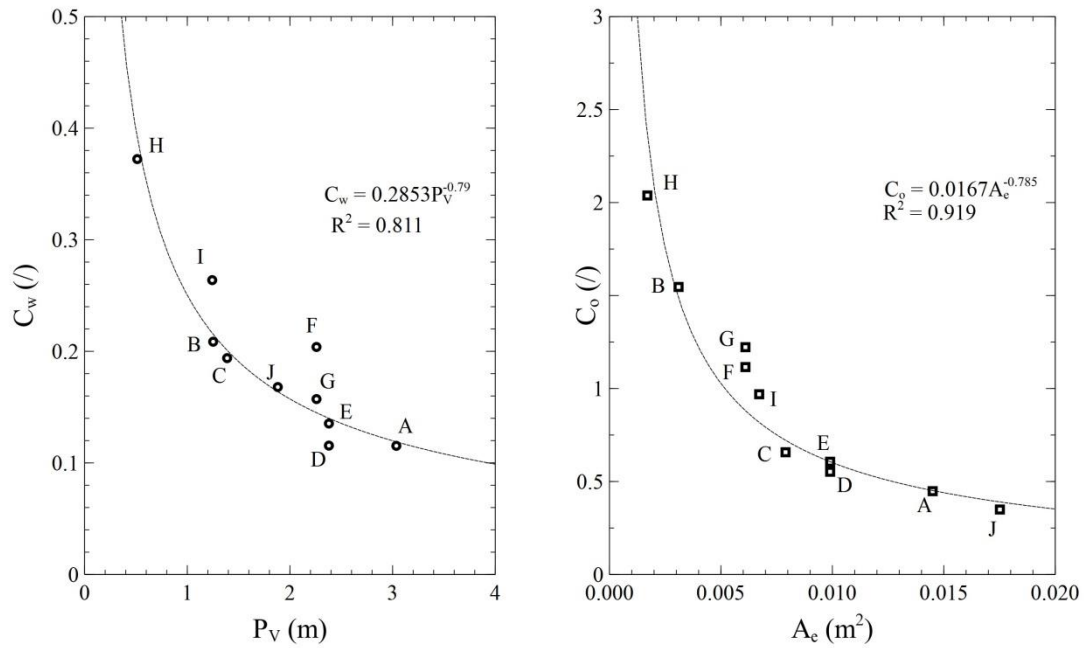
280

281 **Figure 6** | (left) The relationship between the weir equation (3) for each flow condition
 282 tested vs the correspondent flow exchange; (right) the relationship between the orifice
 283 equation (4) vs the correspondent flow exchange.

284 Calibrated discharge coefficients show an inverse trend with the geometrical parameters
 285 (P_v or A_e) associated with the different grate types, suggesting a higher energy loss
 286 associated with surface to sewer flow transfer as opening size decreases (Figure 7).
 287 Figure 7 shows that coefficients approach an approximately constant value ($C_w \approx 0.115$,
 288 $C_o \approx 0.35$ in this case) as opening size and size and perimeter length increases. The
 289 consideration of individual grate types shows that the application of the weir equation
 290 tends to provide higher R^2 values for grate types when the perimeter length value (P_v) is
 291 relatively large (e.g., grate types D and G), while the orifice equation tends to provides
 292 higher R^2 values for grate types when the perimeter length value is smaller (e.g., grate
 293 types B and C). This may be due to the increased likelihood of grates with small
 294 effective perimeters to become ‘drowned’. However, the effect is relatively subtle and
 295 in some cases the difference in R^2 values is negligible even between designs with large
 296 or small effective perimeter values (e.g., grate types A and H).

297 **Table 3** | Values of experimentally calibrated weir and orifice coefficients (C_w and C_o)
 298 and correspondent goodness of fit R^2 values

Grate	C_w	R^2	C_o	R^2
A	0.115	0.984	0.448	0.987
B	0.208	0.951	1.546	0.974
C	0.194	0.985	0.657	0.991
D	0.115	0.957	0.552	0.950
E	0.135	0.995	0.606	0.998
F	0.204	0.981	1.115	0.994
G	0.157	0.995	1.222	0.976
H	0.372	0.966	2.038	0.967
I	0.264	0.989	0.969	0.989
J	0.168	0.969	0.349	0.978



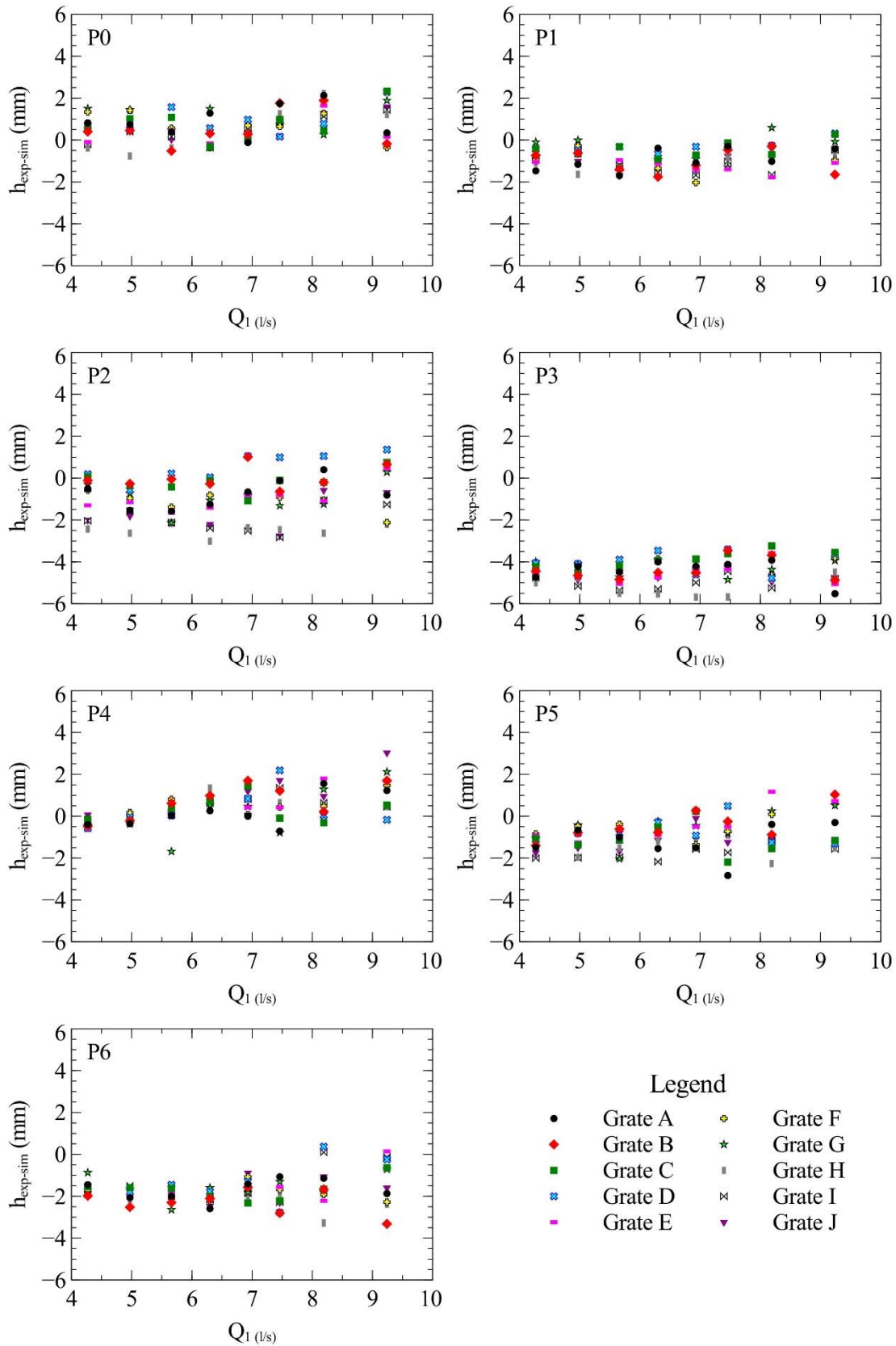
300

301 **Figure 7** | Relationships between experimentally calibrated weir (C_w) and orifice (C_o)
 302 coefficients and geometrical parameters for each inlet grate.

303 Numerical results

304 Figure 8 displays the difference between the experimental depths, as measured by the
 305 transducers (Figure 2), with the depths calculated by the numerical model at each
 306 measurement location ($h_{exp} - h_{sim}$). In most locations the numerical results overestimate
 307 the experimentally observed water depths. At locations P_0 and P_4 (i.e., 75 mm left and
 308 right of the inlet), this condition is reversed and the model tends to underestimate
 309 observed water depths. Despite this, overall, the numerical model provides a good
 310 representation of the experimental observations within the range of 0–5 mm of the
 311 experimental values when considering the full range of inlet flow conditions (Q_1).
 312 Modelling errors may be due to the uncertainties related to: (i) the replication of grates
 313 and the correspondent discretisation of the meshing system adopted; (ii) discrepancies
 314 in the floodplain bed elevation applied within the model; (iii) minor effects due to any
 315 skewed inflow from the inlet tank in the experimental model; (iv) use of the upstream
 316 water depth to calculate total flow exchange instead of actual hydraulic head at each
 317 exchange cell as well as any discharge coefficient calibration errors; (v) the depth
 318 averaged nature of the model or other simplifications. Errors are generally seen to be
 319 smaller for the range of $Q_1 = [4.2; 7.46]$ l/s. By analysing each measurement location

320 separately, P_2 and P_3 (i.e., just upstream and downstream of the inlet) show the highest
321 discrepancies (up to 5 mm). This may be related to complex flow patterns forming
322 upstream and downstream of the inlet (such as water accumulation and separation and
323 merging of stream flows) that the model may find difficult to fully replicate.
324 Discrepancies (0–3 mm) are also noted within the pressure measurement P_6 located 460
325 mm upstream of the centreline of the inlet. For measurement locations less influenced
326 by the flow entering the inlet, such as P_1 and P_5 , errors are within the range 0–2 mm. In
327 terms of flow exchange rate, the numerical simulations tend to overestimate the average
328 exchange discharge (on average by 0.25 l/s). Flow exchange calculations within
329 modelling tools are sensitive to calculations of relative head within pipe and surface
330 systems (Rubinato et al. 2017a). In this case, flow exchange is calculated using the
331 calibrated weir equation based on the numerical simulation of flow depth upstream of
332 the inlet. Resulting discrepancies in the simulation of hydraulic water depths around the
333 inlet can therefore be seen to propagate to the calculation of flow exchange rate.
334



335

336 **Figure 8** | Comparison between the experimental observations and numerical hydraulic

337 heads at each measurement location.

338 **SUMMARY AND CONCLUSIONS**

339 This work has explored the experimental and numerical modelling of surface to sewer
340 flow exchange. A physical model, linking a slightly inclined urban floodplain to a sewer
341 system, was used to carry out measurements under steady state flow conditions with the
342 application of ten different circular grates on the top of a surface/sewer linking
343 structure. Eighty steady state experiments were conducted, during which water levels at
344 seven locations surrounding the inlet structure were measured. The results have
345 confirmed the validity of both the weir and orifice linking equations to describe the total
346 surface to sewer exchange flows through different inlet grates. Calibrated discharge
347 coefficients have been provided for each grate type tested which were taken as constant
348 over the range of hydraulic conditions tested. Overall, the calibrated orifice discharge
349 coefficient showed a larger variation between the grate types. Whilst some evidence
350 was provided to suggest that the weir equation outperforms the orifice equation when
351 the effective perimeter of the grate is relatively high, and vice versa, no significant
352 difference in performance was observed over the range of flow rates tested. Overall
353 trends suggested that discharge coefficients (i.e. energy losses) decrease as the grate
354 geometrical parameters (void area and effective perimeter) increase and may converge
355 to an approximately constant value. In addition, a finite difference numerical model was
356 tailored to reproduce flow conditions around the inlet structure. Experimentally
357 calibrated exchange equations were used to define the inflow through each modelled
358 grate type. The numerical results have been compared with the experiments in terms of
359 depth around the inlet at seven sampling points and detailed comparisons show a regular
360 agreement between the numerical and experimental water levels (maximum discrepancy
361 5 mm). It can therefore be concluded that the proposed 2D numerical approach is able
362 to model floodplain-to-sewer interaction and flow conditions in the vicinity of the
363 linking structure reliably, despite the uncertainties generated by the different geometries
364 of the grates applied and any head variations over the inlet structure. Maximum
365 discrepancies were observed immediately upstream and downstream of the inlet
366 structure, likely due to the complex flow patterns generated by the grate types. While it
367 is not currently feasible to use such methods directly within full scale flood simulations
368 (due to the small mesh sizes required), the work demonstrates the academic capability
369 of the modelling technique and validates the model for supplementary studies. It was
370 also noted that minor discrepancies in the calculation of flow depth propagated to the

371 estimation of flow exchange by the numerical model. Further, more detailed
372 investigation of the exchange flows and the development of modelling approaches that
373 can inherently account for spatially variable energy losses, flow depths and flow
374 exchange rates within different inlet configurations will require characterisation of the
375 velocity fields such that a full understanding of the flow can be elucidated.

376

377 **ACKNOWLEDGEMENT**

378 This research was funded by EPSRC through a grant with the reference EP/K040405/1.
379 The experiments were conducted in the Water Laboratory of the Civil and Structural
380 Engineering Department of the University of Sheffield. Dr. Lee acknowledges the
381 support from the APEC Climate Center.

382

383 **REFERENCES**

- 384 Almedeij, A. O. & Houghtalen, R. J. 2005 Urban Hydrology: Hydraulics and Storm
385 Water Quality. John Wiley & Son, Hoboken, NJ.
- 386 Bazin, P. H., Nakagawa, H., Kawaike, K., Paquier, A. & Mignot, E. 2014 Modeling
387 flow exchanges between a street and an underground drainage pipe during urban
388 floods. *Journal of Hydraulic Engineering* 140 (10), 04014051.
- 389 Chen, A., Djordjevic', S., Leandro, J. & Savic', D. 2007 The urban inundation model
390 with bidirectional flow interaction between 2D overland surface and 1D sewer
391 networks. In: *NOVATECH 2007 – Sixth International Conference on Sustainable
392 Techniques and Strategies in Urban Water Management*, Lyon, France, pp. 465–
393 472.
- 394 Djordjevic', S., Prodanovic', D., Maksimovic', C., Ivetic', M. & Savic', D. 2005
395 SIPSON-simulation of interaction between pipe flow and surface overland flow in
396 networks. *Water Science and Technology* 52 (5), 275–283.
- 397 Djordjevic', S., Saul, A. J., Tabor, G. R., Blanksby, J., Galambos, I., Sabtu, N. & Sailor,
398 G. 2013 Experimental and numerical investigation of interactions between above
399 and below ground drainage systems. *Water Science and Technology* 67 (3), 535–
400 542.
- 401 Gómez, M. & Russo, B. 2009 Hydraulic efficiency of continuous transverse grates for
402 paved areas. *Journal of Irrigation and Drainage Engineering* 135 (2), 225–230.

403 Gómez, M. & Russo, B. 2011a Methodology to estimate hydraulic efficiency of drain
404 inlets. *Proceedings of the Institution of Civil Engineers* 164 (2), 81–90.

405 Gómez, M., Macchione, F. & Russo, B. 2011b Methodologies to study the surface
406 hydraulic behaviour of urban catchments during storm events. *Water Science and*
407 *Technology* 63 (11), 2666–2673.

408 Gómez, M., Hidalgo, G. & Russo, B. 2013 Experimental campaign to determine grated
409 inlet clogging factors in an urban catchment of Barcelona. *Urban Water Journal* 10
410 (1), 50–61.

411 Guo, J. C. 2000a Design of grate inlets with clogging factor. *Advances in*
412 *Environmental Research* 4, 181–186.

413 Guo, J. C. 2000b Street stormwater conveyance capacity. *Journal of Irrigation and*
414 *Drainage Engineering* 72 (5), 626–630.

415 Haleem, D. A., Kesserwani, G. & Caviedes-Voullième, D. 2015 Haar wavelet-based
416 adaptive finite volume shallow water solver. *Journal of Hydroinformatics* 17 (6),
417 857–873.

418 Hammond, M., Chen, A. S., Djordjevic, S., Butler, D. & Mark, O. 2015 Urban flood
419 impact assessment: a state-of-the-art review. *Urban Water Journal* 12 (1), 14–29.

420 Larson, C. L. 1947 Investigation of Flow Through Standard and Experimental Grate
421 Inlets for Street Gutters, Project Report, St. Antony Falls Hydraulic Laboratory,
422 University of Minnesota.

423 Leandro, J., Chen, A., Djordjevic, S. & Savic, D. 2009 Comparison of 1D/1D and
424 1D/2D coupled (sewer/surface) hydraulic models for urban flood simulation.
425 *Journal of Hydraulic Engineering* 135, 495–504. [http://dx.doi.org/10.1061/\(ASCE\)](http://dx.doi.org/10.1061/(ASCE)HY.1943-7900.0000037#sthash.1QracRZb.dpuf)
426 [HY.1943-7900.0000037#sthash.1QracRZb.dpuf](http://dx.doi.org/10.1061/(ASCE)HY.1943-7900.0000037#sthash.1QracRZb.dpuf).

427 Leandro, J., Lopes, P., Carvalho, R., Pascoa, P., Martins, R. & Romagnoli, M. 2014
428 Numerical and experimental characterization of the 2D vertical average-velocity
429 plane at the centre-profile and qualitative air entrainment inside a gully for drainage
430 and reverse flow. *Journal Computer & Fluids* 102, 52–61.

431 Lee, S., Nakagawa, H., Kawaike, K. & Zhang, H. 2013 Experimental validation of
432 interaction model at storm drain for development of integrated urban inundation
433 model. *Journal of Japan Society of Civil Engineers, Ser. B1 (Hydraulic*
434 *Engineering)* 69 (4), 109–114.

435 Lee, S. 2013 Study on Development of Integrated Urban Inundation Model
436 Incorporating Drainage Systems. Ph.D Thesis, Kyoto University.

- 437 Li, W. H., Geyer, J. C. & Benton, G. S. 1951 Hydraulic behaviour of stormwater inlets:
438 I. Flow into gutter inlets in straight gutter without depression. *Sewage and*
439 *Industrial Wastes* 23 (1), 34–46.
- 440 Li, W. H., Goodel, B. C. & Geyer, J. C. 1954 Hydraulic behavior of stormwater inlets:
441 IV. Flow into depressed combination inlets. *Sewage and Industrial Wastes* 26 (8),
442 967–975.
- 443 Lopes, P., Leandro, J., Carvalho, R. F., Páscoa, P. & Martins, R. 2015 Numerical and
444 experimental investigation of a gully under surcharge conditions. *Urban Water*
445 *Journal* 12, 468–476.
- 446 Martins, R., Leandro, J. & Carvalho, R. F. 2014 Characterization of the hydraulic
447 performance of a gully under drainage conditions. *Water Science and Technology*
448 69 (12), 2423–2430.
- 449 Martins, R., Kesserwani, J., Rubinato, M., Lee, S., Leandro, J., Djordjevic´, S. &
450 Shucksmith, J. 2017a Validation of 2D shock capturing flood models around a
451 surcharging manhole. *Urban Water Journal* 14 (9), 892–899. [http://dx.doi.org/10.](http://dx.doi.org/10.1080/1573062X.2017.1279193)
452 [1080/1573062X.2017.1279193](http://dx.doi.org/10.1080/1573062X.2017.1279193).
- 453 Martins, R., Leandro, J., Chen, A. & Djordjevic´, S. 2017b A comparison of three dual
454 drainage models: shallow water vs local inertia vs diffusive wave. *Journal of*
455 *Hydroinformatics* 19 (1). doi:10.2166/hydro.2017.075.
- 456 Rubinato, M. 2015 Physical Scale Modelling of Urban Flood Systems. Ph.D Thesis,
457 University of Sheffield, <http://etheses.whiterose.ac.uk/9270/>.
- 458 Rubinato, M., Seungsoo, L., Kesserwani, G. & Shucksmith, J. 2016 Experimental and
459 numerical investigation of water depths around a manhole under drainage
460 conditions. In: 12th International Conference on Hydroinformatics-Smart Water for
461 the Future, 21–26 August, Songdo Convensia, Incheon, South Korea.
- 462 Rubinato, M., Martins, R., Kesserwani, J., Leandro, J., Djordjevic´, S. & Shucksmith, J.
463 2017a Experimental calibration and validation of sewer/surface flow exchange
464 equations in steady and unsteady flow conditions. *Journal of Hydrology* 552, 421–
465 432. <https://doi.org/10.1016/j.jhydrol.2017.06.024>.
- 466 Rubinato, M., Martins, R., Kesserwani, G., Leandro, J., Djordjevic, S. & Shucksmith, J.
467 2017b Experimental investigation of the influence of manhole grates on drainage
468 flows in urban flooding conditions. In: 14th IWA/IAHR International Conference
469 on Urban Drainage, 10–15 September, Prague, Czech Republic.

- 470 Ten Veldhuis, J. A. E. & Clemens, F. H. L. R. 2010 Flood risk modelling based on
471 tangible and intangible urban flood damage quantification. *Water Science and*
472 *Technology* 62 (1), 189–195.
- 473 Wang, Y., Liang, Q., Kesserwani, G. & Hall, J. W. 2011 A 2D shallow flow model for
474 practical dam-break simulations. *Journal of Hydraulic Research* 49 (3), 307–316.
- 475 Xia, X., Liang, Q., Ming, X. & Hou, J. 2017 An efficient and stable hydrodynamic
476 model with novel source term discretisation schemes for overland flow and flood
477 simulations. *Water Resources Research* 53. doi:10.1002/2016WR020055.
- 478